GaN-based High Frequency 6.6kW Bi-directional DC/DC Converter for OBC Application

Minli.Jia
Electric Vehicle Power Supply Design Department
Navitas Shanghai Design Center
Shanghai, China
minli.jia@navitassemi.com

Hao.Sun
Electric Vehicle Power Supply Design Department
Navitas Shanghai Design Center
Shanghai, China
hao.sun@navitassemi.com

***Abstract*—DAB (Dual-active-bridge) and CLLC are two common isolated bidirectional DC/DC converters, but they are limited by soft switching and gain adjustment range respectively, and cannot meet the requirements of high-efficiency, bidirectional, wide range, and full power transmission of products. Boost-SRC is a combination of the advantages of the two, using vary frequency and phase-shift control method, meet the soft switch, the higher gain and suitable for wide output voltage regulation applications. In this paper, firstly, the working principle of the topology is introduced, and the time domain analysis is carried out based on the phase-plane analysis method. Secondly, the general engineering design steps and system control methods are given. Finally, a 6.6kW bidirectional DC/DC prototype was built using Navitas Nano-Toll packaging GaN devices, and the charge and discharge efficiency curves were measured, the highest switching frequency up to 900khz，which verified the feasibility of GaN devices application in high-power vehicle products.**

Keywords—Bi-directional DC/DC, On-board-charger(OBC), GaN devices, Boost-SRC

I. INTRODUCTION

Bidirectional isolated DC/DC converter is the main energy conversion unit of bidirectional OBC of EVs and is a research hotspot in recent years. DAB and CLLC are two representative bidirectional topologies with their own advantages and disadvantages. Since the publication of literature [1], the academic circle has carried out a large number of studies on DAB focusing on its limited soft switching range [2,3]. DAB is a fixed-frequency PWM control in nature. Most of the studies focus on using multi-phase shifting control methods to expand its soft switching range and improve conversion efficiency, but the control is relatively complex. There are other literatures that reduce loop circulation by adding auxiliary circuits [4], but the system cost increases. CLLC is a resonant converter, using vary-frequency modulation control, full range ZVS switching, but for wide voltage bidirectional applications, it is difficult to design the system gain. In literature [5,6], variable Bus voltage is adopted to realize the output of wide voltage, which ensures that most of the output voltage works near quasi resonant. The reactive power circulation is smaller, and the efficiency is higher, but it brings pressure to the AC/DC control of the front stage and increase the volume of bus capacitance.

By absorbing the advantages of DAB and CLLC, Boost-SRC (Series-Resonant-Converter) adopts vary-frequency and phase-shift control method, which has the characteristics of switching ZVS action, high gain and wide voltage output. This topology was first proposed in literature [7] as an application of unidirectional wide voltage range output. Based on bidirectional application, the delay-time control method was proposed in literature [8], and the control and gain characteristics of this topology were studied in detail to expand its application field.

GaN power devices, as the third-generation semiconductor [9], are characterized by high switching frequency, low on-resistance and zero reverse charge recovery compared with traditional Si devices. In addition, with the maturity of silicon-based GaN transistors and other production processes, the cost of silicon-based GaN has rapidly decreased, and the cost performance has gradually improved. GaN power devices have achieved preliminary industrialization and large-scale application in consumer electronics and other fast charging source adapters. In the future, it will have broad application prospects in data center, server power supply, solar power generation, electric vehicle charging and discharging, green energy storage and other medium-high power occasions [10].

II. TOPOLOGY AND WORKING PRINCIPLE ANALYSIS

A. Topology and moduletion strategy

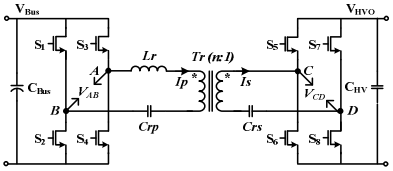

Fig. 1. Boost-SRC circuit topology

The circuit topology of bidirectional Boost-SRC is shown in Fig. 1. *S1~S8* are power switches. *Lr* is resonant inductance; Tr is an isolation transformer with turn ratio of *n :1*; *Crp* and *Crs* are the resonant capacitors of the primary and secondary, respectively. *CBus* and *CHV* are Bus and output side capacitors respectively. As LC series resonance, no need excitation inductor, *Lr* position can be flexibly configured. This paper takes *Lr* in the primary side as an example for analysis.

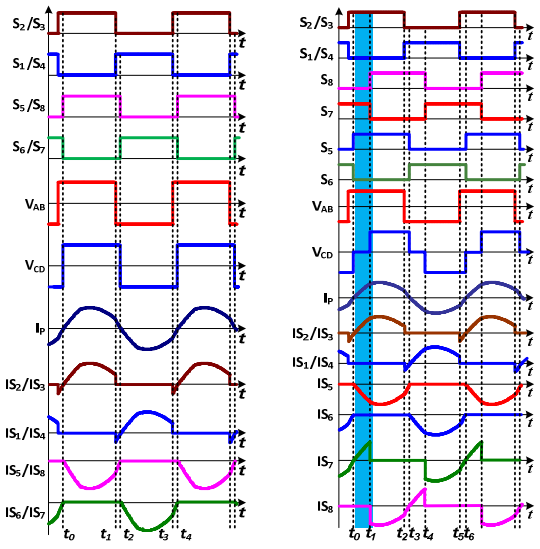

(a) Gain<1 (b) Gain>1

Fig. 2. Modulation strategy and typicle waveforms

978-1-6654-9141-9/22/$31.00 ©2022 IEEE

According to the working principle of delay-time control (also known as phase-shift control) [8]. The two adjacent switches in *S5~S8* can be randomly selected for synchronous rectification control and the other two for phase-shift control. In this paper, *S5* and *S6* are selected for synchronous rectification control and *S7* and *S8* for phase-shift control.

B. Working mode analysis

Assuming that the dead time of the drive signal is zero, only the positive half cycle differential gain is analyzed according to the symmetry of the resonant circuit.

When the Gain is less than 1, Boost-SRC works in the Vary-Frequency state, and the output voltage regulates with the switching frequency, Fig. 2 (a) is the corresponding modulation method. It can be seen that there are two working modes in half a switching cycle [*t0*, *t2*].

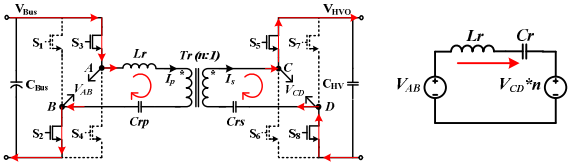

(a) Mode 1 (b) Equivalent circuit

Fig. 3. Working mode 1 and its equivalent circuit

Working mode 1 [*t0*, *t1*] (Fig. 3): before the *t0*, *S2*/*S3* are ZVS turn on, and then the resonant current changes from negative to positive. The primary side voltage *VBus* excites the resonant tank, and *S5*/*S8* synchronous rectification charges the *CHV*. Fig. 3(b) is the corresponding equivalent circuit.

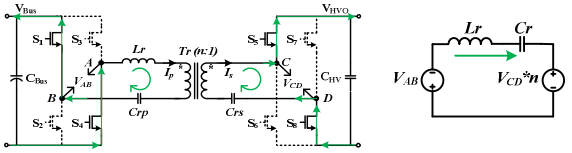

(a) Mode 2 (b) Equivalent circuit

Fig. 4. Working mode 2 and its equivalent circuit

Working mode 2 [*t1*, *t2*] (Fig. 4) : At *t1*, *S2*/*S3* is turn off and *S1*/*S4* is ZVS turn on. On the one hand，the resonant current feeds energy to the primary side, which will create soft switching conditions for the primary side devices, and on the other hand, transfer energy to the output load. The equivalent circuit is shown in Fig. 4(b).

When the gain is more than 1, the switching sequence is shown in Fig. 2 (b), and the [*t1*, *t2*] and [*t2*, *t3*] correspond to working modes 1 and 2 respectively, without further details. Only the additional modes are analyzed below.

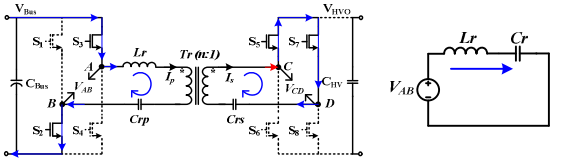

(a) Mode 3 (b) Equivalent circuit

Fig. 5. Working mode 3 and its equivalent circuit

Working mode 3 [*t0*, *t1*] (Fig. 5): *S2*/*S3* is on state. At *t0*, *S5* is ZVS turn on and because of *S7* is delayed to turn off, resonant current is continued through *S5* and *S7* to store energy for resonant inductor. During this time， *VBus* excites the resonant tank，transformer secondary side is short, hence the Boost-SRC name. The equivalent circuit is shown in Fig. 5(b).

In short，there are three working modes, mode 1 is normal power transmission; Mode 2 is the energy feedback stage, providing ZVS working conditions; Mode 3 is the core of the circuit, which can improve the gain of output voltage.

C. Phase plane analysis

The principle of phase plane method was proposed by Poincare in 1885. It is a graphical method as well as a time-domain analysis method, which can not only analyze the stability and self-excited oscillation of the system, but also clearly display the motion track of the system. The method can also analyze linear and nonlinear systems. The brief analysis is as follows：

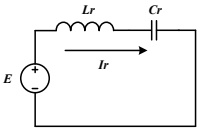

Fig. 6. Series LC resonance circuit

The KVL equation in Fig. 6 is as follows:

$$L_r \frac{di_{Lr}}{dt} + u_{Cr} = E \tag{1}$$

Also because $C_r * du_{Cr}/dt = i_{Lr}$, equation (1) can also be expressed as:

$$L_r C_r \frac{d^2 u_{Cr}}{dt^2} + u_{Cr} = E \tag{2}$$

Suppose the initial state of the circuit is $U_{Cr}(0) = U_{Cr0}$,$i_{Lr}(0) = 0$, $\omega_r = 1/\sqrt{L_r C_r}$. By solving the differential equations for equations (1) and (2), the resonant voltage and current can be expressed as follows：

$$u_{Cr} = (u_{Cr0} - E)cos\omega_r t + E \tag{3}$$

$$i_{Lr} = \sqrt{\frac{C_r}{L_r}}(u_{Cr0} - E)sin\omega_r t \tag{4}$$

From the previous analysis, the equivalent circuits (mode 1,2 and 3) of the above are LC series resonance, so phase-plane method can be used to analyze and study them. *Cr* is the equivalent resonant capacitance and satisfy $Cr = Crp(Crs/n^2)/(Crp + Crs/n^2)$; Characteristic impedance: $R_0 = \sqrt{Lr/Cr}$; Angular frequency: $\omega = 1/\sqrt{LrCr}$; All parameters are normalized based on *VBus* as follows：

- Input voltage：$M_g = V_{Bus}/V_{Bus} = 1$
- Output voltage：$M_g = V_{HVO}n/V_{Bus}$
- Voltage of *Cr*：$m_c = V_{CR}/V_{Bus}$
- Peak voltage of *Cr*：$M_{RP} = V_{CR_{PEK}}/V_{Bus}$
- Current of the resonant tank：$j_L = i_{Lr}R_0/V_{Bus}$

When gain <1, the equivalent circuit are Fig. 3 (b) and Fig. 4 (b), and the corresponding phase-plan is shown in Fig. 7. The horizontal axis is defined as the resonant current, the vertical axis is defined as the resonant capacitor voltage. At *t0*, the resonant current is zero, and the voltage of resonant capacitor reaches its maximum value *MRP*. The excitation source of the resonant tank in the period [*t0*, *t1*] is *Mg-M*, and

the phase-plane moves counterclockwise with (*0*, *Mg-M*) as the center of the circle and *R2* as the radius until *t1*, and the arc angle corresponding to this period is β. The excitation source in the period of [*t1*, *t2*] becomes *-Mg-M*, and an arc with angle γ is made with (0, *-Mg-M*) and *R3* as the radius, so as to complete phase-plane drawing of half a period.

Where, $d1=2Mg$, $R2=MRP+Mg-M$, $R3=MRP+M+Mg$.

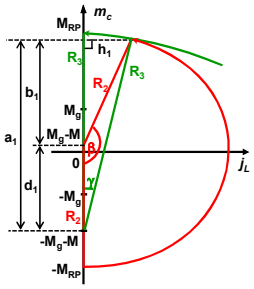

Fig. 7. Phase-plan of half switching period with gain <1

According to geometric relations, the following expressions can be obtained:

$$\begin{cases} a_1 - b_1 = d_1 \\ a_1^2 + h_1^2 = R_3^2 \\ b_1^2 + h_1^2 = R_2^2 \end{cases} \tag{5}$$

a1 and *h1* can be calculated from (5):

$$a_1 = \frac{R_3^2 - R_2^2 + d_1^2}{2d_1} \tag{6}$$

$$h_1 = \sqrt{R_3^2 - a_1^2} \tag{7}$$

The angles of β and γ can be calculated as follows

$$\gamma = \sin^{-1}\frac{h_1}{R_3} \tag{8}$$

$$\beta = \cos^{-1}\frac{R_2^2 + d_1^2 - R_3^2}{2R_2 d_1} \tag{9}$$

Where, angle β and γ satisfy: $\gamma + \beta = \pi$. The action time of β Angle is defined as $T\beta$, and the resonant current expression of gain <1 is as follows:

$$I_{Lr}(t) = \begin{cases} \frac{V_g}{R_0}[R_2 \sin(\omega t)] & 0 \le t < T_\beta \\ \frac{V_g}{R_0}\{R_3 \sin[\beta + \omega(t - T_\beta)]\} & T_\beta \le t \le \frac{T_s}{2} \\ -\frac{V_g}{R_0}\left[R_2 \sin\left(\omega\left(t - \frac{T_s}{2}\right)\right)\right] & \frac{T_s}{2} < t \le \pi + T_\beta \\ -\frac{V_g}{R_0}\left\{R_3 \sin\left[\beta + \omega\left(t - \frac{T_s}{2} - T_\beta\right)\right]\right\} & \frac{T_s}{2} + T_\beta < t \le T_s \end{cases} \tag{10}$$

According to formula (10), the waveform of a period can be obtained as shown in Fig. 8. The corresponding working periods of angle β and γ in the half cycle are marked.

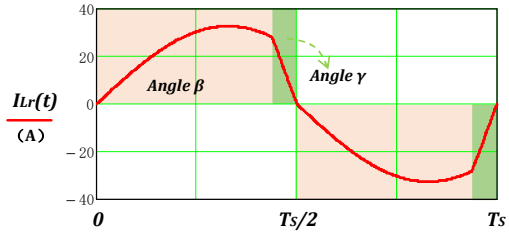

Fig. 8. Resonant current waveform of a *Ts* when gain <1

The phase-plane with gain >1 is shown in Fig. 9 which is divided into two cases according to the size of *a2* and d2. The equivalent circuit in Fig. 5(b) is added, and its corresponding angle is defined as α. The drawing method is the same as described above and will not be detailed.

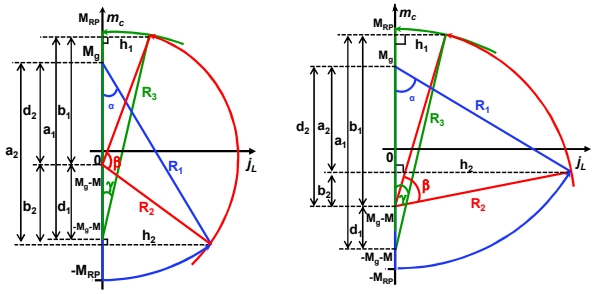

(a) a2>d2 (b) a2<d2

Fig. 9. Phase plan of half switching period with gain >1

According to the phase-plan of Fig. 9(a),$d1=2Mg$, $d2=M$, $R1=MRP+Mg$, $R3=MRP+M+Mg$. According to geometric relations, the same expressions as equations (5)~(8) can be solved, and other expressions are also as follows:

$$\begin{cases} a_2 - b_2 = d_2 \\ a_2^2 + h_2^2 = R_1^2 \\ b_2^2 + h_2^2 = R_2^2 \end{cases} \tag{11}$$

$$a_2 = \frac{R_1^2 - R_2^2 + d_2^2}{2d_2} \tag{12}$$

$$h_2 = \sqrt{R_1^2 - a_2^2} \tag{13}$$

The α Angle can be obtained as:

$$\alpha = sin^{-1}\frac{h_2}{R_1} \tag{14}$$

β starting Angle is:

$$\beta_{start\_angle} = sin^{-1}\frac{h_2}{R_1} \tag{15}$$

α, β and γ angles satisfy:

$$\beta = \pi - sin^{-1}\frac{h_2}{R_1} - sin^{-1}\frac{h_1}{R_3} \tag{16}$$

When the gain >1, the expression of inductance resonance current is:

$I_{Lr}(t) =$

$$\begin{cases} \frac{V_g}{R_0}[R_1 \sin(\omega t)] & 0 \le t < T_\alpha \\ \frac{V_g}{R_0}\{R_2 \sin[\omega(t - T_\alpha) + \beta_{start\_angle}]\} & T_\alpha \le t < T_\alpha + T_\beta \\ \frac{V_g}{R_0}\{R_3 \sin[\omega(t - T_\alpha - T_\beta) + \pi - \gamma]\} & T_\alpha + T_\beta \le t \le \frac{T_s}{2} \\ -\frac{V_g}{R_0}\left[R_1 \sin\omega\left(t - \frac{T_s}{2}\right)\right] & \frac{T_s}{2} \le t < \frac{T_s}{2} + T_\alpha \\ -\frac{V_g}{R_0}\left\{R_2 \sin\left[\omega\left(t - \frac{T_s}{2} - T_\alpha\right) + \beta_{start\_angle}\right]\right\} & \frac{T_s}{2} + T_\alpha \le t < \frac{T_s}{2} + T_\alpha + T_\beta \\ -\frac{V_g}{R_0}\left\{R_3 \sin\left[\omega\left(t - \frac{T_s}{2} - T_\alpha - T_\beta\right) + \pi - \gamma\right]\right\} & \frac{T_s}{2} + T_\alpha + T_\beta \le t \le T_s \end{cases} \tag{17}$$

The waveform of a period can be obtained according to formula (17), as shown in Fig. 10. The corresponding working periods of angle α, β and γ in the half cycle are marked.

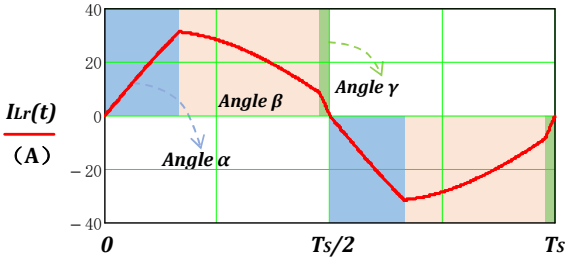

Fig. 10. Resonant current waveform of a Ts when gain >1

When the α angle is larger, the working condition as shown in Fig. 9 (b) will occur, and its relation is the same as that in Fig. 9 (a), without detailed explanation. The difference is that the starting angle of β Angle under Fig. 9 (b) working condition is:

$$\beta_{start\_angle} = \pi - sin^{-1}\frac{h_2}{R_1} \tag{18}$$

D. Angle γ design consideration when Gain>1

It can be known from working mode 3 that the γ angle is closely related to the realization of switch ZVS. At $t1$, the resonant current flows to the devices capacitor $Coss$ of the two switches to charge. To realize the soft switch, the inductance current and capacitor voltage energy must meet the following equation:

$$\frac{1}{2}L_r i_{Lr}(t_1)^2 \geq 2 * \frac{1}{2}C_{OSS}{V_{Bus}}^2 \tag{19}$$

The minimum current satisfying the switch ZVS is:

$$i_{Lr\_ZVS\_Min} = V_{Bus}\sqrt{2\frac{Coss}{Lr}} \tag{20}$$

So the minimum $h1$ expression after normalization is as follows:

$$h_1 = \frac{i_{Lr\_ZVS\_Min}R_0}{V_{Bus}} \tag{21}$$

So far, under the condition of known $Coss$ capacitance value, γ angle can be calculated. In meeting the ZVS switching requirements, Angle γ should be as small as possible to reduce the reactive power loss of the system.

E. Gain curve and characteristic analysis

The gain expression of the Boost-SRC topology is described in detail in reference [8], which is directly referenced in this paper. The charging and discharging gain curves of 6.6kW Boost-SRC are shown in Fig. 11 (a) and (b), including different output voltage points.

It can be seen that the ratio of switching frequency to resonant frequency is greater than 1 and the larger the phase-shift angle, the greater the gain. The dashed line shows the working track at different output voltages and show "V" type. Compared with LLC control, its switching frequency range is narrower, which is conducive to the optimal design of magnetic components.

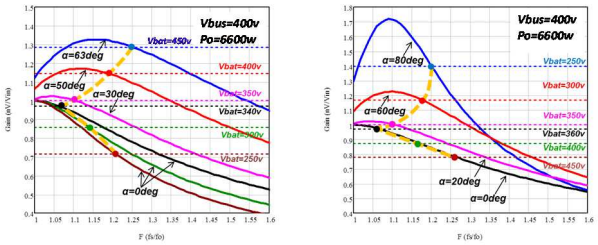

(a) Charging mode (b) Discharging mode

Fig. 11. Gain curve of charging and discharging mode

III. SYSTEM DESIGN STEPS AND CONTROL

A. Resonant tank design steps

Step 1: Determine the peak value of the resonant capacitor (VCr_pek) according to the voltage withstand of the selected resonant capacitor. For example, if the resonant capacitor with a withstand voltage of 630V is selected, 80% safety margin is considered, and the value of VCr_pek is 267V.

Step 2: The lowest output voltage point is usually designed near the quasi-resonant point. Under this condition, the voltage of the resonant capacitor is the highest, and the energy between capacitor voltage and inductance current meets the relation of $Cr*VCr=ILr*t$, that is:

$$C_r = \frac{\frac{1}{n}I_{o\_Max}}{2V_{Cr\_pek}} \times \frac{T_r}{2} \tag{22}$$

Where, Io_Max is the average current at full load output, Tr is the resonant period.

Step 3: When the Cr and fr are determined, the Lr value can be calculated as follows:

$$L_r = \frac{1}{(2\pi f_r)^2 C_r} \tag{23}$$

Step 4: For the application of wide output voltage, the transformer's turn ratio design should ensure that it works in quasi-resonant state near the lowest output voltage point as far as possible, so as to reduce reactive power loss and improve efficiency.

$$n = \frac{V_{Bus}}{V_{HVO\_normal}} \tag{24}$$

Where, $VHVO\_normal$ is the minimum output voltage within the rated voltage range.

B. System control

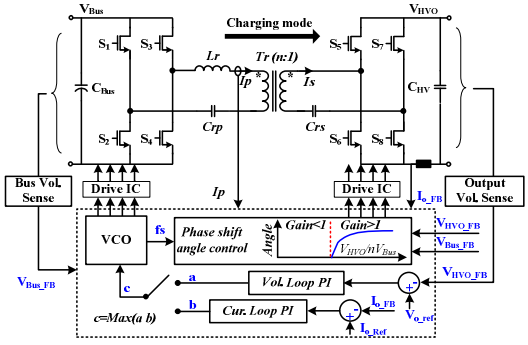

Fig. 12. Boost-SRC system control block

The control block diagram of the system is shown in Fig. 12. Input voltage, resonant current, output voltage and current are sampled respectively.

It has constant voltage and constant current control. The switching frequency and the phase-shift angle of the primary and secondary sides are two control variables of the system. The former is controlled by closed-loop, while the latter is realized by open-loop table lookup. The phase-shift angle meets a certain functional relationship with the input and output voltage (expression 25) and can be obtained by means of testing.

$$Angle_{\alpha} = f(V_{Bus},\ V_{HVO}) \tag{25}$$

Under the condition of the same output voltage, the switching frequency is changing, but the angle of phase-shift is constant, so the digital control is easy to realize.

IV. System Parameter Design and Verification

A. Main parameters design

A 6.6kW bi-directional DC/DC converter is designed for EV On-board-charger. The main performance parameters are shown in Table I.

TABLE I. 6.6kW BI-DC/DC MAIN PARAMETERS

	6.6kW Bi-DC/DC	
	Electronic Spec.	Value
Electronic SPEC.	VBus	380~420V
	V_{HVO}	280~460V for full load
	Power	6.6kW for charger and 6.3kW for discharger
Resonance parameters	Resoanter inductor	4.0uH
	Resonant cap.	40nF (Equivalent)
	Resonant frequency	400khz

In the battery voltage range of 280~460V, 6.6kW for charging and 6.3kW for discharging. The resonant frequency is 400khz, and according to the characteristics of the Boost-SRC circuit mentioned above, its actual operating frequency will be above 400khz.

B. GaN device and characteristics

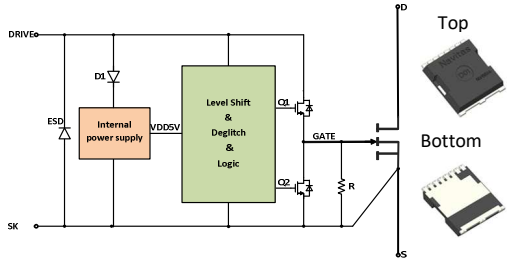

Fig. 13. Control block of NV6514

NV6514, the latest generation of Nano-Toll-packaged GaN semiconductor device of Navitas, is selected as the main power device in this paper. As shown in Fig. 13, Its internal integrated with 5V power supply unit can provide power for the internal logic circuit, level shift and deglitch circuit for Improve anti-interference performance. The introduction of these functions can reduce the parasitic parameters of the drive loop, inhibit the crosstalk phenomenon, and improve the reliability of GaN. In addition, the drive voltage of 8~20V makes the device easy to use and design.

TABLE II. MAIN PARAMETERS OF NV6514

Navitas NV6514	
Electronic Spec.	Value
Rds(on)	25 m Ω @25℃
Ids_continuous	85A@25℃
Coss	129pF @400V，Vgs=0V
E_on /	110uJ@Vds=400V,Ids=30A, Rg=1Ω
E_off	20uJ@ Vds=400V,Ids=30A
Qrr	0

Main parameters of NV6514 are shown in Table II. Si-IGBT with the same current level and SiC devices with the same Rds(on) are selected to compare with NV6514. Fig. 14 shows the comparison curves of *Eon* and *Eoff*. It can be seen that NV6514 has obvious advantages *Eon* and *Eoff,* which means that GaN devices have low switching losses and are suitable for high switching frequency applications.

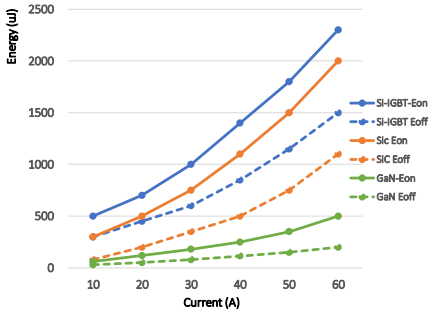

Fig. 14. Comparison between Eon and Eoff

C. Experimental protopyte and results

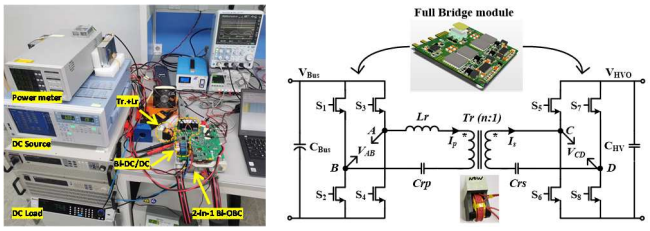

Fig. 15. Experimental prototype

The experimental prototype of bidirectional DC/DC is shown in Fig. 15. The power unit adopts modular design, which is convenient for maintenance and installation. The Integrated transformer was designed which further reduce the volume and improve the power density.

Fig. 16. Charging mode (380VBus-280VHVO)

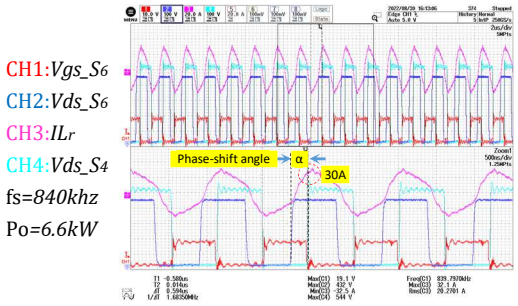

Fig. 17. Charging mode (420VBus-460VHVO)

Fig. 16 and 17 show the switching waveforms of 280V and 460V output respectively in charging mode. It can be seen that with the addition of angle α, the output gain and voltage are increased, and the switching frequency is up to 840khz.

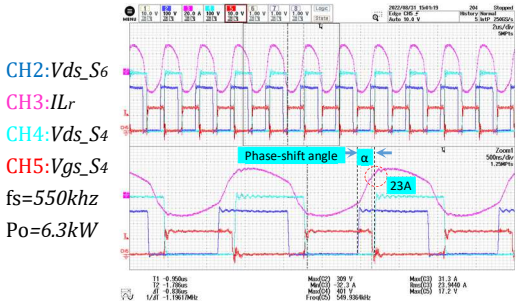

Fig. 18. Discharging mode (280VHVO-380VBus)

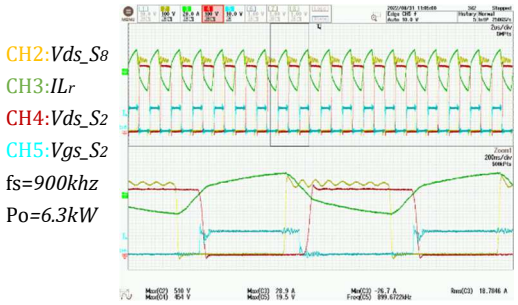

Fig. 19. Discharging mode (460VHVO-420VBus)

Fig. 18 and 19 show the switching waveforms of 280V and 460V input respectively in discharging mode. It can be seen that with the addition of angle α, the output gain and voltage are increased at 280V battery voltage. The highest switching frequency is up to 900khz when the battery is 460V.

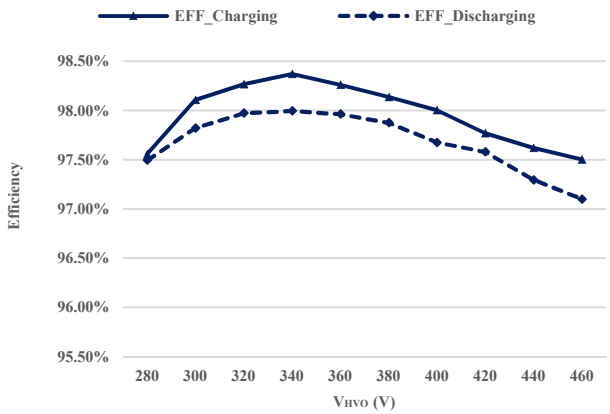

Fig. 20. Charge and discharge efficiency curve

Fig. 20 shows the final test efficiency. It can be seen that the highest efficiency in charging and discharging mode is 98.4% and 98%, respectively. The lowest efficiency of the system is above 97%. In the discharging mode, due to the wide voltage range is operated in the vary-frequency mode, its efficiency is about 0.3% lower than that of the charging mode, as a results of the high switching-off loss and reactive current loss.

V. SUMMARY

Bidirectional Boost-SRC with ZVS switching, wide gain, high frequency and high efficiency characteristics, suitable for electric vehicle battery charging applications in a wide voltage range; Its resonance parameters design simple, *Lr* and *Cr* are designed and configured flexibly; Combined with the low switching loss characteristics of GaN devices, the switching frequency of the Bi-DC/DC can be further increased, so as to reduce the volume of the transformer and further improve the power density of the product.

Next, the converter efficiency will be further optimized, and the high temperature endurance test will be completed to further verify the performance of Navitas GaN devices.

ACKNOWLEDGMENT

The authors would like to thank all Engineers from the Power Electronics Laboratory, Navitas Shanghai EV team, for their assistance in constructing and programming the experimental converter.

REFERENCES

[1] Kheraluwala M N, Gascoigne R W. Performance characterization of a high-power dual active bridge DC-to-DC converter[J]. IEEE Trans Industry Applications, 1992, 28(6):1294-1301.

[2] Shao S, Chen H, Wu X, et al. Circulating Current and ZVS-on of a Dual Active Bridge DC-DC Converter: A Review[J]. IEEE Access, 2019, 7:50561-50572.

[3] Carvalho, Edivan Laercio, et al. "Asymmetrical-PWM DAB converter with extended ZVS/ZCS range and reduced circulating current for ESS applications." IEEE Transactions on Power Electronics 36.11 (2021): 12990-13001.

[4] Zhao B, Song Q, Liu W, et al. Overview of Dual-Active-Bridge Isolated Bidirectional DC–DC Converter for High-Frequency-Link Power-Conversion System[J]. IEEE TRANSACTIONS ON POWER ELECTRONICS PE, 2014, 29(8):4091-4106.

[5] Li B, Lee F C, Qiang L, et al. Bi-directional on-board charger architecture and control for achieving ultra-high efficiency with wide battery voltage range[C]// Applied Power Electronics Conference & Exposition. IEEE, 2017.

[6] Zou S, Lu J, Mallik A, et al. Bi-Directional CLLC Converter with Synchronous Rectification for Plug-In Electric Vehicles[J]. IEEE Transactions on Industry Applications, 2018, 54(2):998-1005.

[7] Rossetto L, Spiazzi G. Series Resonant Converter with Wide Load Range[C]// Conference Record-ieee Industry Applications Meeting. IEEE, 1998.

[8] Liu G, Jang Y, Jovanovic M, et al. Implementation of a 3.3-kW DC–DC Converter for EV On-Board Charger Employing the Series-Resonant Converter with Reduced-Frequency-Range Control[J]. IEEE Transactions on Power Electronics, 2017, 32(6):1-1.

[9] Jones E A, Fei F W, Costinett D. Review of Commercial GaN Power Devices and GaN-Based Converter Design Challenges[J]. IEEE Journal of Emerging & Selected Topics in Power Electronics, 2016, 4(3):707-719.

[10] T. Van Do, J. P. F. Trovão, K. Li and L. Boulon, "Wide-Bandgap Power Semiconductors for Electric Vehicle Systems: Challenges and Trends," in IEEE Vehicular Technology Magazine, vol. 16, no. 4, 2021, pp. 89-98.